Defence Science Journal, Vol. 71, No. 6, November 2021, pp. 721-729, DOI : 10.14429/dsj.71.16468

Active Flow Control over a NACA23012 Airfoil using Hybrid Jet

Deepak Kumar Singh[@], Anuj Jain[#], and Akshoy Ranjan Paul[#,*]

[@]*Department of Applied Mechanics, Indian Institute of Technology Delhi, New Delhi - 110 016, India*
[#]*Department of Applied Mechanics, Motilal Nehru National Institute of Technology Allahabad, Prayagraj - 211 004, India*
[*]*E-mail: arpaul2k@gmail.com*

ABSTRACT

A time-dependent numerical simulation is performed to examine the flow separation control with the action of a hybrid jet (the combination of synthetic and continuous jets) over a NACA23012 airfoil. The unsteady Reynolds-averaged Navier–Stokes (URANS) simulation is performed with Spalart-Allmaras (SA) turbulence model to simulate the flow field around the airfoil to analyse the effect of the hybrid jet. A combined jet is placed at the point of flow separation on the upper surface of the airfoil which is located at the 12% of the chord length from the leading edge of the airfoil for a given flow configuration. Flow simulations are performed at a chord-based Reynolds number of 2.19×10^6 for the hybrid jet oscillating frequency of 0.159 at a blowing ratio of 3.0. The contribution of the continuous jet in the hybrid jet is evident by the flow control. Variation in the continuous jet velocity is studied, which improved the aerodynamic characteristics of the airfoil. The maximum improvement in lift to drag ratio is observed from 11.19 to 22.14 at an angle of attack of 22 degree. The stall angle also shows an enhancement from 18 degree to 20 degree.

Keywords: Active flow control; Airfoil; Synthetic jet; Continuous jet; Hybrid jet

NOMENCLATURE

A	Axial force on the airfoil
AoA	Angle of attack
α_j	Inclination angle of a jet from the airfoil surface
B	Blowing ratio of the jet $\left(=V_j / U_\infty\right)$
C_l	Coefficient of lift
C_d	Coefficient of drag
C_p	Pressure coefficient
C_μ	Momentum coefficient $\left(=\rho V_j^2 h / q_\infty c\right)$
c	Chord length of the airfoil
D	Total drag force on the airfoil
f	Jet actuation frequency
$f(\eta)$	Velocity distribution
f_j^+	Dimensionless frequency of jet $\left(=xf / U_\infty\right)$
H	Synthetic jet throat width
L	Lift force on the airfoil
LE	Leading edge of the airfoil
N	Normal force on the airfoil
p	Pressure
R	Non-dimensional mean velocity $\left(=U_{mean} / U_\infty\right)$
Re	Reynolds Number
T	Time
TE	Trailing edge of the airfoil
U_{mean}	Mean velocity of the hybrid jet
U_∞	Free-stream velocity
V_j	Amplitude of synthetic jet velocity
x_j	Distance from the jet location to the LE
α	Angle of attack
χ	Distance from the jet location to the TE

Received : 05 November 2020, Revised : 22 January 2021
Accepted : 22 February 2021, Online published : 22 October 2021

1. INTRODUCTION

The aerodynamic characteristics of the wing are adversely affected by the flow separation on the wing, especially at the high angles of attack. The flow separation over the wing is a very complex phenomenon and it depends on the various geometrical parameters of the airfoil and flow conditions of the airplane. The geometrical parameters of an airfoil are depending on various parameters such as camber line, thickness distribution, and so on. Many researchers reported the effects of geometrical parameters on the aerodynamic coefficient of various airfoils. However, the flow conditions such as the angle of attack (AoA), Reynolds number (Re), Mach number, etc. have significant effects on the aerodynamic performance of an airfoil. At low Reynolds number (less than 5×10^5) and a moderate range of angles of attack, the laminar boundary layer starts separating on the upper surface of an airfoil near the leading edge, undergoes a transition, and subsequently rapid reattachment of the separated shear layer takes place. But at the higher Reynolds number in order of 5×10^5 to 9×10^6 the turbulent boundary layer separation occurs. In the past several decades, many researchers[1-5] worked on high Reynolds number ranges. The flow over an airfoil in this range of Reynolds number and for a wide angle of attack plays a crucial role in the aerodynamic coefficients which are summarised below:

- At low angles of attack, the rate of increment in lift coefficient is greater than the drag coefficient. The flow starts separating near the trailing edge (Pre-stall condition) with an increasing angle of attack.
- As the value of the angle of attack increases in a moderate

range, the lift coefficient increases and finally attains maximum lift condition. The corresponding angle of attack is called stall angle and this type of flow condition is called stall condition. At this condition, the point of separation lies near the trailing edge of the airfoil (Stall condition).

- At post-stall, the angle of attack increases, and the lift coefficient starts reducing drastically. This flow condition is called the post-stall condition. At this condition, the point of flow separation lies near the leading edge of the airfoil (post-stall condition).

The aerodynamic performance decreases when the boundary layer separates over an airfoil and flow control is required to maintain attached flow. The control of this boundary layer separation is always a fascinating topic for researchers.

Many flow control techniques are classified based on the usage of an external source of energy. The active flow control mechanism requires an external source of energy for actuation. But in the passive flow control mechanism, there is a need for an external source of energy. The present study is focused on the active flow control mechanism to control turbulent boundary layer separation.

Huang[2], *et al.* performed a numerical study on flow separation control over a NACA0012 airfoil at AoA= 18° using a continuous jet and conducted parametric analysis on the position of the jet, amplitude, and angle of inclination of the jet. Wong and Kotnis[4] studied flow separation control on a similar airfoil with a continuous jet placed at the LE, quarter chord from the LE and the TE, and the various AoA ranging from −20° to 20°. Yousefi[5], *et al.* found effects of blowing and suction on a similar airfoil at a chord-based Reynolds number of 5x10^5 and various angles of attack.

In recent years, flow control by synthetic jets are studied extensively[6-12] and it is seen as an effective method for flow separation control over an airfoil. The synthetic jet flow control technique can add/remove enough momentum to the boundary layer to prevent the flow separation without adding any net mass flow rate. The flow control over an airfoil using the synthetic jets is affected by the following parameters:

- Dimensionless frequency of the jet, $\left(F_j^+ = xf / U_\infty\right)$.
- The ratio of the synthetic jet velocity amplitude to the free-stream velocity of the flow, $\left(= V_j / U_\infty\right)$;
- Reynolds number and the Mach number of the flow.
- Blowing momentum coefficient, $\left(= \rho V_j^2 h / q_\infty c\right)$

In recent years, many researchers performed parametric studies of synthetic jets for flow separation control over an airfoil. Buchmann[1], *et al.*, Duvigneau[13], *et al.*, Duvigneau and Visonneau[14] performed a URANS study to control flow separation using synthetic jets. They studied the effects of a jet, located at the x_j=0.12c over a NACA0015 airfoil. Numerical simulation was performed at Re=8.96×10^6 and AoA=12° and 24°. Optimum control parameters suggested from the study were $V_j / U_\infty = 1.72$, $F_j^+ = 0.748$ and a_j=25°.

Kim and Kim[15] performed a URANS study over a NACA 23012 airfoil using synthetic jets flow control technique at Reynolds number =1.2 ×10^6. The synthetic jet was located at the x_j=0.12c and the inclination angle was a_j=23°. It was observed that the optimum location of the jet is the same as the flow separation point for an uncontrolled case.

Monir[3], *et al.* used a finite volume-based solver to perform a URANS study over a NACA23012 airfoil by using a synthetic jet flow control technique at Reynolds number =2.19×10^6. The synthetic jet located at the x_j=0.12c was the same as taken by Kim and Kim[15]. Monir[3], *et al.* recommended the tangential synthetic jet (a_j=0°) and found the following parameters for the optimal control for this configuration: B=3 and a_j=0°.

Nishibe[16], *et al.* performed the experimental study on the effect of the dimensionless stroke length (non-dimensionalised by the slot width) on the synthetic jet at a Reynolds number of 1800. The dimensionless stroke length shows a significant impact on the synthetic jet parameters that have a strong influence on the flow separation control by using these jets.

Feng[17], *et al.* performed numerical simulation over an airfoil S809 at Reynolds number Re=1×10^6. In this study, the synthetic jet flow separation control mechanism is applied over an airfoil at various angles of attack. A study of dual jets is replaced by the single jet and their comparison is also shown in this study. They also found the synthetic jet flow control technique very effective in the higher AoA, especially near the stall angle. The ratio of lift to drag coefficients observed a marked improvement near the stall condition.

The literature review summarised in Table 1 reveals that the continuous and synthetic jets were separately investigated to control flow separation in the airfoils. However, both methods have their advantages and limitations. For example, continuous jet being a simple blowing mechanism adds constant mass flow rate into the system, but it is sometimes considered disadvantageous, especially when the aerodynamic performance is sensitive to mass flow rates. On the other side, synthetic jets, being zero net mass flux jet, do not add any net mass into the system. In the case of synthetic jets, a pair of vortex formed for two-dimensional flow that promotes more momentum mixing as compared to the continuous jets for an airfoil[17]. The flow control using the combined continuous jet and the synthetic jet was, however, not studied.

The above discussion has encouraged the present authors to explore the potential of combined use of blowing and synthetic jets, termed in this paper as a hybrid jet which has not been studied to date. In the present study, the effects of the shifting of the mean velocity of the hybrid jet are analysed, which is characterised by a non-dimensional parameter, R, and the effects of the hybrid jet on the aerodynamic performance characteristics over a NACA23012 airfoil for a wide range of AoA is presented.

The advantages of continuous and synthetic jets are combined in the present study to computationally investigate the lift improvement mechanism of a NACA23012 airfoil. All parameters taken for this study are the same as Monir[3], *et al.* except velocity distribution of the jet. The hybrid jet results are compared with the results of the synthetic jet alone. Besides, the influence of the mean velocity of the hybrid jet in the flow control is also studied. Mathematically, the synthetic jet has zero mean velocity. Numerical analysis is carried out to reveal the influence of the mean velocity of the continuous jet on the aerodynamic performance of the airfoil.

Table 1. Summary of previous work

Authors	Airfoil, Jets, and Reynolds number	Major claims
Buchmann[1] *et al.*	NACA0015. ZNMF jet. Re=3×10⁴	Stall angle increased from 12° to 17°, C_l increased by 47%
Huang[2] *et al.*	NACA0012. Blowing and suction. Re=5×10⁵	Optimised jet location, amplitude, and the angle at α=18⁰.
Monir[3] *et al.*	NACA23012. Synthetic Jets. Re=2.19×10⁶	C_l/C_d is increased by 62% for a tangentially located jet.
Wong and Kontis[4]	NACA0012. Synthetic jet	Spanwise steady blowing increased C_l.
Yousefi[5] *et al.*	NACA0012. Blowing and suction. Re=5×10⁵	Jet widths of 3.5% to 4% of the chord are found most effective for a tangential jet.
Alstrom[6]	NACA0015 with flap at AoA=16°. Synthetic jet array	Three active flow control strategies are investigated to facilitate steep climbing.
De Giorgi[8] *et al.*	NACA0015. Synthetic jet, Continuous jet	The synthetic jet is found better than the continuous jet.
Tuck and Soria[9]	NACA0015. Micro ZNMF jets. Re=1.54×10⁴	Stall angle increased from 10° to 18°, C_l increased by 46%.
You and Moin[10]	NACA0015. Synthetic jets. Re=8.96×10⁵	Stall angle increased from 12° to 18°, C_l increased by 58%.
Duvigneau[13] *et al.*; Duvigneau and Visonneau[14]	NACA0015. Synthetic jets. Re=8.96×10⁶	Stall angle increased from 19° to 22°, C_l increased by 34%.
Kim and Kim[15]	NACA23012 combined with slat and flap. Synthetic jet. Re=1.2×10⁶	Jet frequency is found to be important while using multi-array synthetic jets.
Feng[17] *et al.*	S809. Synthetic jet. Re=1×10⁶	Dual jets are replaced by the single jet at various AoA.

2. COMPUTATIONAL METHODS

2.1 Computational Domain

The computational domain of the airfoil extends from 8-times chord length towards upstream and 12-times chord length towards downstream from the trailing edge of the airfoil. The upper and lower boundary of the flow domain extends 8-times chord length from the airfoil trailing edge as shown in Fig. 1.

2.2 Grid Generation

A simple structured mesh is generated with 166809 computational nodes and 167289 computational elements finalised after the grid independency test. The first wall spacing in the grid is set according to the value of Y^+=1. The grid used

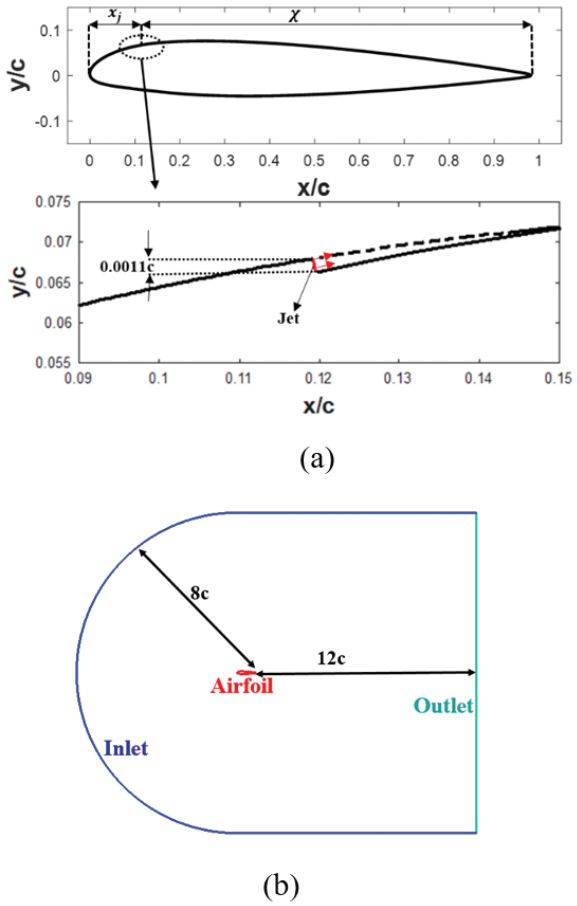

Figure 1. Geometry and computational domain: (a) NACA23012 airfoil with tangential jet location and (b) Computational domain of airfoil and the boundary condition.

for numerical simulations for controlled (with hybrid jets) and uncontrolled (without hybrid jets) cases are generated by the Ansys-ICEM meshing tool and is shown in Fig. 2.

2.3 Governing Equations

Finite volume method-based CFD solver Ansys-Fluent is used for the simulation carried out in the study. Assumptions made in the numerical formulation are the two-dimensional, time-dependent turbulent flow throughout the domain, viscous dissipation is insignificant, and the temperature is constant. Based on these assumptions, the

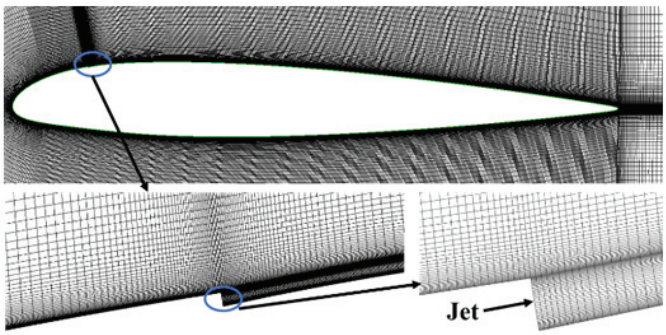

Figure 2. Grid distribution near the airfoil.

governing equations are furnished below:

Equation of continuity:

$$\frac{\partial \rho}{\partial t} + \nabla.(\rho u) = 0$$

Equations of momentum:

X-momentum equation

$$\rho \frac{Du}{Dt} = -\frac{\partial p}{\partial x} + \nabla.(\mu \nabla u)$$

Y- Momentum equation

$$\rho \frac{Dv}{Dt} = -\frac{\partial p}{\partial y} + \nabla.(\mu \nabla v)$$

2.4 Boundary Conditions

The boundary conditions used in the present study are the same as those used in Monir[3], *et al.* everywhere except for the jet profile. The time-dependent velocity profile for the hybrid jet is given below:

$$\vec{U} = \vec{U}_{mean} + V_j \sin(2\pi t) f(\eta) \vec{d}_{jet}$$

where $f(\eta)$ is taken 1 as per Monir[3], *et al*. and $\vec{d}_{jet}$ is a unit vector that shows the jet direction. The time-dependent jet velocity profile obtains by the user-defined function (UDF). The detailed boundary conditions specified for each zone are furnished in Table 2. In the case of a hybrid synthetic jet, $\vec{U}_{mean}$ is the velocity contribution from a continuous jet, while $V_j \sin(2\pi t) f(\eta) \vec{d}_{jet}$ is the contribution from the synthetic jet. The combined velocity $\vec{U}$ is specified at the outlet of the hybrid jet.

Table 2. Boundary conditions

Zone	Type	Boundary condition
Inlet	Velocity Inlet	Free stream velocity magnitude: 32.64 m/s Inlet pressure: 101325 Pa (atmospheric) Temperature=300K
Outlet	Pressure outlet	Outlet pressure: 101325 Pa (atmospheric) Temperature=300K
Jet	Velocity outlet	Velocity magnitude and direction: $\vec{U} = \vec{U}_{mean} + V_j \sin(2\pi t) f(\eta) \vec{d}_{jet}$
Airfoil	Wall	No-slip condition

2.5 Turbulence Models

Spalart-Allmaras (S-A) turbulence model proposed by Spalart and Allmaras[21] is used in the present study. All computations of the present study are performed on a finite volume method-based commercial solver Ansys-Fluent[18]. Literature[3,19-24] shows that the S-A turbulence model offers significantly good computational results closer to the experimental data. In the S-A turbulence model, one transport equation is solved for variable modified turbulent viscosity ($\tilde{\upsilon}$). The $\tilde{\upsilon}$ is equal to turbulent viscosity (υ_t) except in the viscous region. The governing equation of this model:

$$\frac{D(\tilde{\upsilon})}{Dt} = \text{prduction} + \text{diffusion} - \text{dissipation}$$

The governing equation is solved for $\tilde{\upsilon}$ field and then calculate υ_t field by multiplying the viscous damping function f_{v1} as follows.

$$\upsilon_t = \tilde{\upsilon} f_{v1}$$

where, $f_{v1} = \frac{\chi^3}{\chi^3 + C_{v1}^3}$, $\chi \equiv \frac{\tilde{\upsilon}}{\upsilon}$, and C_{v1} is a specified constant and ν is kinematic molecular viscosity.

The production term in the S-A model is modelled as:

$$\text{prduction} = C_{b1} \tilde{S} \tilde{\upsilon}$$

where

$$\tilde{S} = S + \frac{\tilde{\upsilon}}{\kappa^2 d^2} f_{v2}, \; f_{v2} = 1 - \frac{\chi}{1 + \chi f_{v1}}, \; \kappa = 0.41$$

and cell wall distance represented by the *d*. The measure of deformation tensor (*S*) is as:

$$S = \sqrt{2\Omega_{ij}\Omega_{ij}}$$

where

The diffusion term is modelled as

$$\text{diffusion} = \frac{1}{\sigma}\left[\nabla.((\upsilon + \tilde{\upsilon})\nabla\tilde{\upsilon}) + C_{b2}(\nabla\tilde{\upsilon})^2\right]$$

where σ and C_{b2} are constants.

Dissipation term is modelled as

$$\text{destruction} = C_{w1}\left(\frac{\tilde{\upsilon}}{d}\right)^2$$

where C_{w1} is a constant.

This modelled dissipation term produces accurate results in the log layer. But in the outer region of the turbulent boundary layer, it decays too slowly. In the resolution of this deficiency, multiply by a newly modelled function f_w. The value of the f_w in the log layer is

$$\text{dissipation} = C_{w1} f_w \left(\frac{\tilde{\upsilon}}{d}\right)^2.$$

where

$$f_w = \left[\frac{1 + C_{w3}^6}{g^6 + C_{w3}^6}\right]^{1/6}, \; g = r + C_{w2}(r^6 - r),$$

$$r \equiv \frac{\tilde{\upsilon}}{\tilde{S}\kappa^2 d^2}, C_{w2}$$

and C_{w3} are constant.

The convergence criteria for all the governing equations solved is fixed and the scaled residuals to decrease to 10^{-6}.

2.6 Grid Independency Test

Grid generation assumes a significant role in numerical simulation. For grid independence study, a relatively coarse grid with finer near-wall gridding around the airfoil surface is generated in case-1 keeping AoA=18°. The value of the aerodynamic coefficients (C_l and C_d) for case-1 are 1.3815 and 0.09214, respectively. Further grid refinement is carried out and the values of C_l and C_d are monitored as furnished in Table 3 and Fig. 3 until it becomes almost constant. From case-3 to case-4, no significant changes in aerodynamic coefficients are observed. Hence, the grid demonstrated in case-3 is considered for all the simulations.

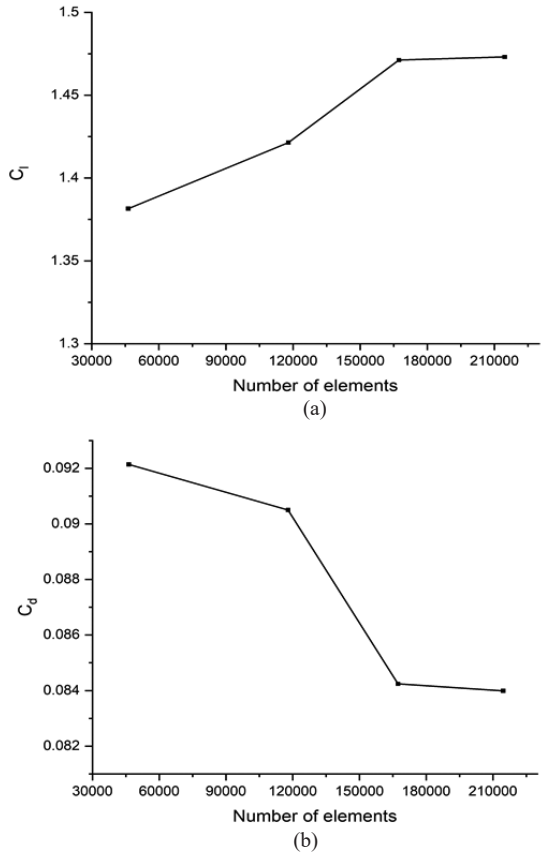

Figure 3. GIT at AoA= 18°: (a) Lift coefficient and (b) Drag coefficient.

Table 3. GIT at AoA= 18°

	Number of elements	C_l	C_d
Case-1	46358	1.3815	0.09214
Case-2	117894	1.4214	0.090501
Case-3	167289	1.4712	0.08424
Case-:4	214570	1.4731	0.08399

3. RESULTS AND DISCUSSIONS

In this section, the convergence of the solution and validation of the results are presented. Besides, parametric studies on the effect of the mean of the velocity of the hybrid jet are also presented, which is characterised by a non-dimensional parameter, $R= U_{mean}/U_{\infty}$. The value of R varies from 0 to 1 and analyses the influence of the R on aerodynamic characteristics.

3.1 Convergence

For the unsteady simulation, the numerical solution must be converged in the time-space as well. For the time convergence in the present study, the time-step is calculated based on the hybrid jet cycle. A jet cycle is divided into 360-time steps and each time step has 500 sub iterations. The final time step size becomes $\Delta t=f\times 1/360 \times 1/500=5.5\times 10^{-6} f$ sec, which is the order of CFL number 1. At every time-step, the solution is converged to the order of 10^{-6}. After the tenth jet cycle, the solution becomes quasi-steady in nature. Hence, the solution is extracted after the tenth jet cycle.

3.2 Validation

In the present study, flow over NACA23012 airfoil is validated with Monir[3] *et al.* taking the same dimensions and same flow conditions. Airfoil is tested at a Reynolds number of 2.19×10^6 corresponding to the free stream velocity of 32.64 m/s over a wide range of AoA in controlled cases. In the validation, B=3 and F_j^+=0.159 are used. The maximum Mach number in this study is 0.4 observed. The variation of lift coefficient versus AoA is shown in Fig. 4 (a) while drag coefficient versus AoA is shown in Fig. 4 (b). The variation in lift and drag coefficients as compared to the results reported in Monir[3], *et al.* lie within 7%, which is considered reasonable to proceed for further analysis.

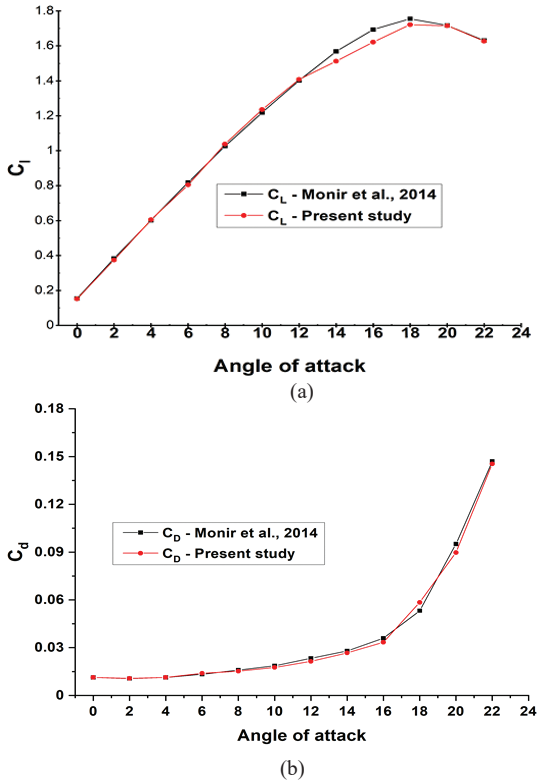

Figure 4. Validation of present work: (a) Lift coefficient vs. angle of attack and (b) Drag coefficient vs. angle of attack.

3.3 Streamlines over the Airfoil

Figure 5 presents the flow streamlines over the airfoil coloured with the ratio of velocity magnitude to the free stream velocity at AoA = 22° without any hybrid jet control. It clearly shows the boundary layer separation occurs near the leading edge of the airfoil.

The streamlines with the controlled cases are compared with the uncontrolled cases. Figure 6 shows the streamlines over airfoil for controlled cases with $R= U_{mean}/U_{\infty}$ =0 and 1. The streamlines in Fig. 6 are coloured with the ratio of velocity magnitude to free stream velocity at an angle of attack 22°. A jet cycle is divided into eight equal phases.

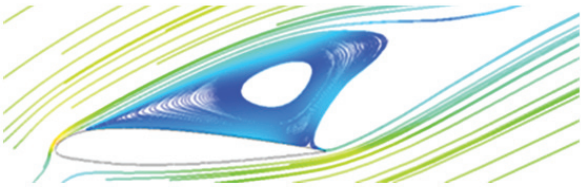

Figure 5. Time-averaged streamlines over the airfoil at AoA= 22° without jet control (refer to the legend of Fig. 6).

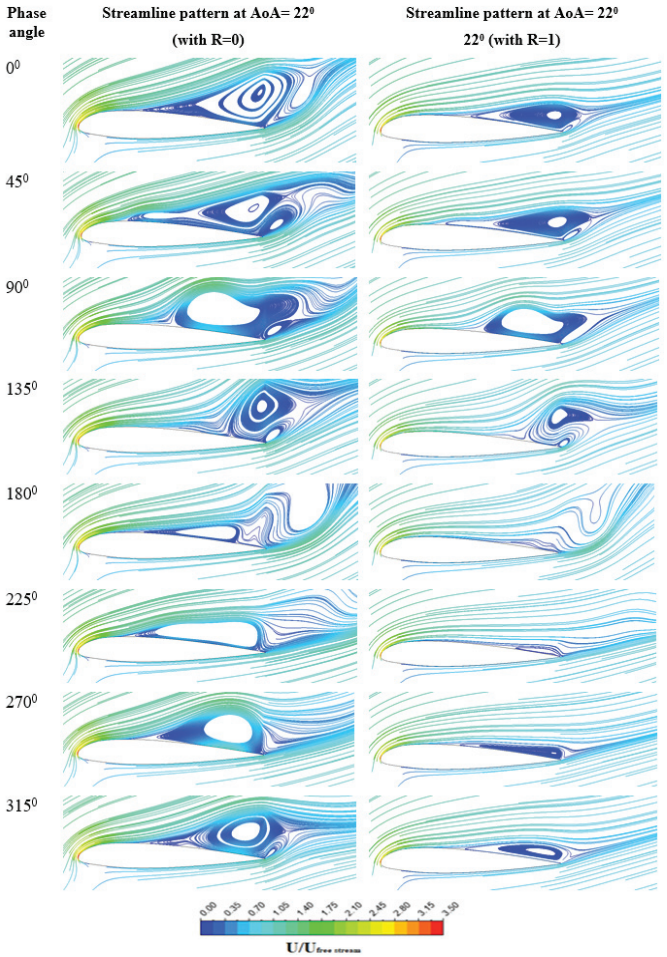

Figure 6. Comparison of flow streamlines at R=0 and R=1 over the airfoil.

Referring to Fig. 6 at phase angle 0°, a larger primary vortex appears on the upper surface of the airfoil at R=0 compared to the R=1. The vortex size is reduced in the case of R=1 and the flow separation point also appears downstream compared to the R=0. At a phase angle of 45°, a secondary vortex appears at the trailing edge of the airfoil in both cases. At this instant, the secondary vortex becomes smaller in the case of R=1. The secondary vortex convected by the primary vortex is shown at a phase angle 90°. But the primary vortex core is shifted slightly upstream. At a phase angle of 135°, the primary vortex is convected downstream and subsequently appears near the trailing edge of the airfoil. The point of flow separation moves downstream in both cases.

For a phase angle of 180°, the primary vortex starts to form on the upper surface of the airfoil in case of R=0, while for R=1, flow is fully attached signifying the effects of the value of R. Afterwards, the primary vortex shows rapid growth in the next phases for R=0. The size of the primary vortex is also larger compared to the R=1.

The effect of the mean velocity in hybrid jet shows a significant improvement in flow features. Increasing the value of R helped in reducing the flow separation region as well as the vortex size behind the airfoil. Aerodynamic coefficients show a significant improvement in Figs. 9-11.

3.4 Time History of Aerodynamic Characteristics

The time history of the aerodynamic coefficients over the airfoil shown in this section, compared the aerodynamic coefficients by the flow separation control by the synthetic jet (R=0) and hybrid jet (R=1) to that of an uncontrolled case. Mathematically, a synthetic jet has zero mean of velocity, so the effects of the mean of the velocity of the jet are investigated in this section.

A time history of the aerodynamic coefficients during seven jet cycles of the synthetic jet at the AoA=22° is presented in Fig. 7-8, where time is taken in terms of several cycles. The final lift and drag coefficients reported in this study are the time-averaged value at a particular AoA.

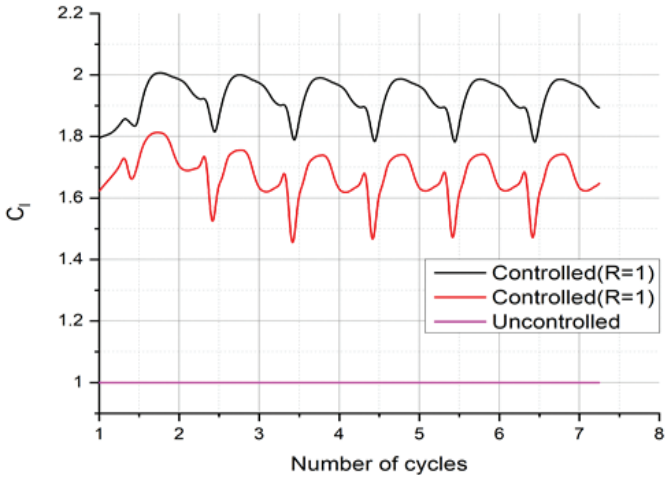

Figure 7. Time history of lift coefficient of (C_l) at AoA= 22°.

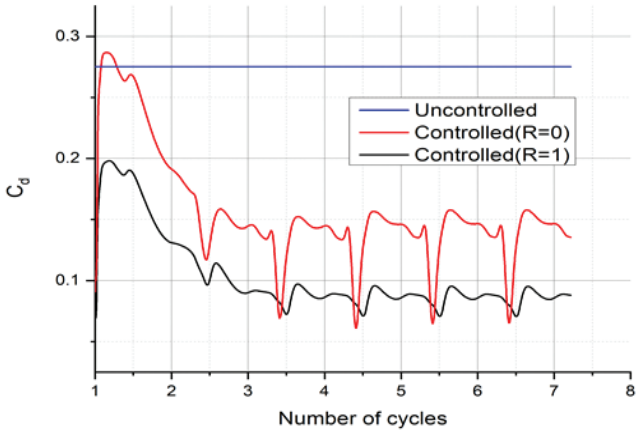

Figure 8. Time history of co-efficient of drag (C_d) at AoA= 22°.

Figure 7 clearly shows that the lift coefficient is enhanced in the case of the hybrid jet (R=1). After two cycles, the lift coefficient follows the same cyclic pattern. The value of C_l is increased much from the uncontrolled case at R=1. The lift coefficient is directly proportional to R for pre-stall conditions, which is evident in Fig. 9.

On the other hand, the drag coefficient is reduced in the case of the hybrid jet (R=1) as depicted in Fig. 8. It clearly shows that after 3 cycles, the drag coefficient follows the same cyclic pattern. At the phase angle of 180°, the value of C_d is minimum indicating the most favorable condition in terms of the drag reduction. It is also shown in Fig. 6, where at phase angle=180°, the flow separation point reaches almost at the trailing edge. At R =0, fluctuation in C_d is much higher than the case of R=1 as noticed in Fig. 8.

3.5 Effect of R on Lift Coefficient of Airfoil

Figure 9 presents the lift coefficient versus AoA at different values of R. The value of C_l is increased with increment in R. The stall angle is also increased with the values of R and is shown in Table 4. It is worthwhile to note that the stall angle in the uncontrolled case is 16°.

Table 4. Value of *R* and corresponding stall angle

Value of *R*	Stall angle of the airfoil
0	18°
0.2	19°
0.6	19°
1	20°

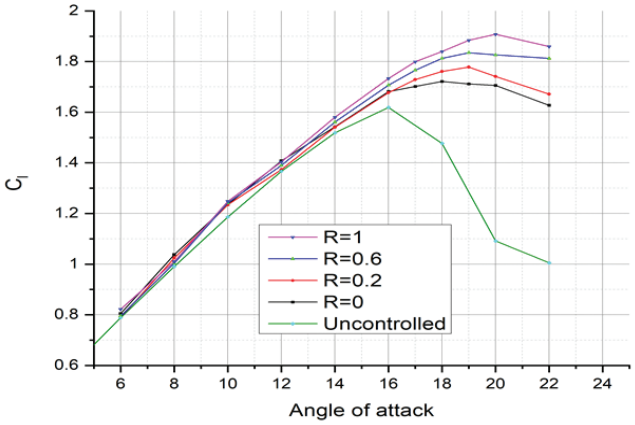

Figure 9. Effect of *R* on lift coefficient of the airfoil.

3.6 Effect of R on Drag Coefficient of the Airfoil

Figure 10 represents the C_d versus AoA at different values of R. The value of C_d is decreased with the increase of R. In the case of R=1 and at AoA=22°, the drag coefficient is reduced by 50% from the value corresponding to R=0. At the higher AoA, the hybrid jet is found more effective related to low values of angles of attack.

3.7 Effect of *R* on C_l/C_d of the Airfoil

Figure 11 presents the effect of R on C_l/C_d of airfoil over an entire angle of attack. At the higher values of AoA,

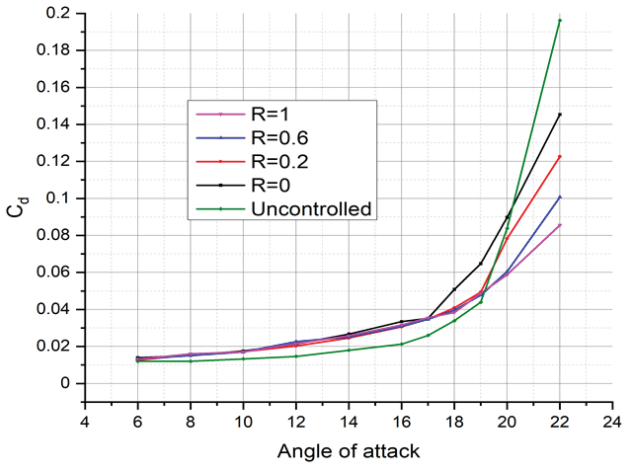

Figure 10. Effect of *R* on the drag coefficient of the airfoil.

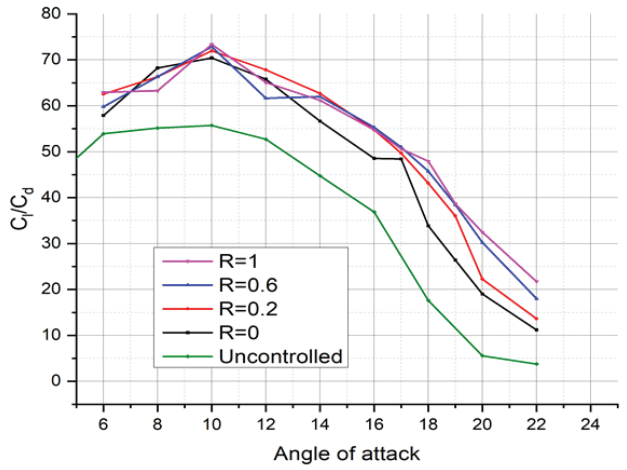

Figure 11. Effect of *R* on C_l/C_d of the airfoil.

the hybrid jet is proved more effective related to low values of AoA which is clearly shown in Fig. 11. Hybrid jet is more effective at AoA=22°, where the value of C_l/C_d is increased by 100% (from C_l/C_d=11 at R=*0* to C_l/C_d=22 at R=*1*).

From Fig. 11, it shows that before AoA= 16°, the flow control using jet is not proved much effective because the flow separation point is not adjacent to the jet location. At AoA= 16°, the flow separation point is just away from the jet location as discussed in sub-section 3.3 in an uncontrolled case. Then jet control is found much effective at AoA= 16° and even beyond it. This is evident from Figs. 9-11.

3.8 Contours of Dimensionless *z*-vorticity

Contours of z-vorticity ($\omega_z\ c/U_\infty$) for the uncontrolled and controlled case at AoA=22° are shown in Fig. 12. In an uncontrolled case, a shear layer starts to separate near the leading edge of the airfoil around (x/c=0.12) which is the same as the Monir[3], *et al.* The shear layer, however, does not have a significant amount of turbulence level to ensure reattachment on the upper surface of the airfoil and the shear layer eventually forms a strong wake region behind the airfoil. In the controlled case for R=1, the flow separation of the shear layer is delayed by the additional momentum applied by the hybrid jet. The flow separation occurs further downstream as compared to the uncontrolled case as clearly shown in Fig. 12.

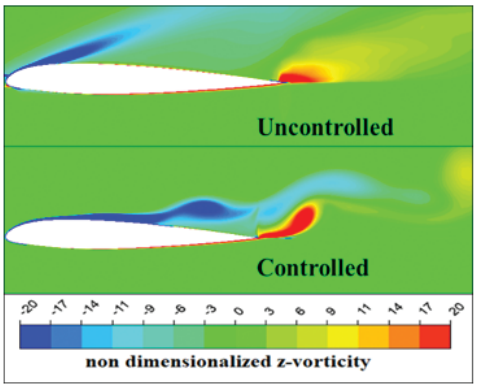

Figure 12. Contours of *z*-vorticity ($\omega_z c/U_\infty$) for the uncontrolled and controlled cases at AoA=22°.

The flow separation does not form a strong wake behind the airfoil as shown in Fig. 6, but an attached flow is observed over most of the part of the airfoil. A vortex shedding is observed behind the airfoil at AoA= 22° which is shown in Fig. 13. For the uncontrolled case, the flow separation starts near the leading edge of the airfoil which is shown in Fig. 13, and forms a large pair of vortex behind the airfoil. But in the controlled case (R=1), the flow separation shifted downstream and eventually formed a small pair of vortices as compared to the uncontrolled case.

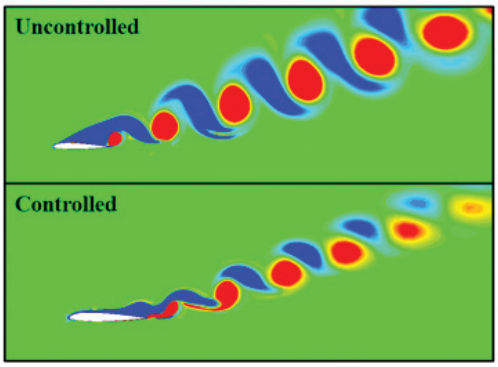

Figure 13. Vortex shedding behind the airfoil at AoA= 22°.

3.9 Contours of Turbulent (eddy) Viscosity Ratio

Contours of turbulent (eddy) viscosity ratio, which is the turbulent viscosity normalised by the molecular viscosity of the fluid is shown in Fig. 14 for both the uncontrolled and controlled cases (R=1). A massive separated region is observed over the airfoil from the contours of the turbulent viscosity ratio in an uncontrolled case. The separated region in the controlled case is however smaller and shifted downstream of the airfoil.

4. CONCLUSIONS

In the current study, control of the flow separation by the action of a hybrid jet is carried out and the effects of the mean velocity of the hybrid jet are also analysed. The following conclusions are made from the present study.

- Flow separation point moves towards trailing edge with the increment in the value of the mean velocity of the jet defined by a non-dimensional parameter, R.

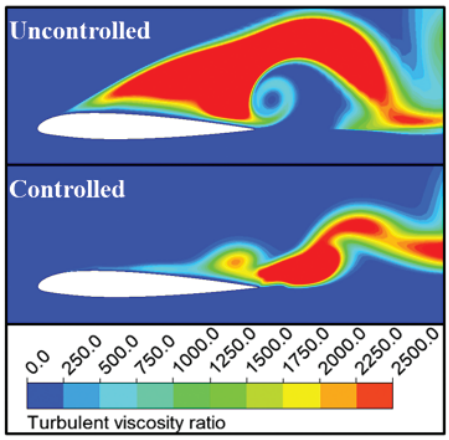

Figure 14. The contour of instantaneous turbulent viscosity ratio at AoA= 22°.

- Aerodynamic characteristics C_l/C_d shows a significant improvement as the value of R increases beyond AoA=16°.
- Stall angle also shows a significant increment with the value of R. At R=0, stall angle is 18° and at R=1, stall angle is 20°.
- A local maximum value of aerodynamic performance observed at AoA=22° is C_l/C_d=11.19, at R=0, which becomes almost doubled C_l/C_d=22.14 for R=1. A tangential synthetic jet with R=1 (termed as hybrid jet) is hence found most efficient.

REFERENCES

1. Buchmann, N.A.; Atkinson, C. & Soria, J. Influence of ZNMF jet flow control on the spatio-temporal flow structure over a NACA0015 airfoil. *Experiments in Fluids*, 2013, **54**(3), 1485. doi: 10.1007/s00348-013-1485-7
2. Huang, L.; Huang, P.G.; LeBeau, R.P. & Hauser, T. Numerical study of blowing and suction control mechanism on NACA0012 airfoil. *Journal of Aircraft*, 2004, **41**(5), 1005-1013. doi: 10.2514/1.2255
3. Monir, H.E.; Tadjfar, M. & Bakhtian, A. Tangential synthetic jets for separation control. *J. Fluids Struct.*, 2014, **45**, 50-65. doi: 10.1016/j.jfluidstructs.2013.11.011
4. Wong, C. & Kontis, K. Flow control by spanwise blowing on a NACA 0012. *Journal of Aircraft*, 2007, **44**(1), 337-340. doi: 10.2514/6.2006-3676
5. Yousefi, K.; Saleh, R. & Zahedi, P. Numerical study of blowing and suction slot geometry optimization on NACA0012 airfoil. *J. Mech. Sci. Technol.*, 2014, **28**(4), 1297-1310. doi: 10.1007/s12206-014-0119-1
6. Alstrom, R. B. Aerodynamic flow control of a high lift system with dual synthetic jet arrays. 2013, *PhDT,* Clarkson University, USA.
7. Cater, J.E. & Soria, J. The evolution of round zero-net-

mass-flux jets. *J. Fluid Mech.*, 2002, **472**, 167.
doi: 10.1017/S0022112002002264

8. De Giorgi, M.G.; De Luca, C.G.; Ficarella, A. & Marra, F. Comparison between synthetic jets and continuous jets for active flow control: Application on a NACA 0015 and a compressor stator cascade. *Aerospace Sci. Technol.*, 2005, **43**, 256-280.
doi: 10.1016/j.ast.2015.03.004
9. Tuck, A. & Soria, J. Separation control on a NACA0015 airfoil using a 2D micro ZNMF jet. *Aircraft Eng. Aerospace Technol.,* 2008.
doi: 10.1108/00022660810859391
10. You, D. & Moin, P. Active control of flow separation over an airfoil using synthetic jets. *J. Fluids Structures*, 2008, **24**(8), 1349-1357.
doi: 10.1016/j.jfluidstructs.2008.06.017
11. Murugan, T.; Deyashi, M.; Dey, S.; Rana, S.C. & Chatterjee, P. Recent developments on synthetic jets. *Def. Sci. J.*, 2016, **66**(5), 489-498.
doi: 10.14429/dsj.66.9776
12. Yadav, K.R.; Paul, A.R.; Hegde, N. & Jain, A. A comparison of circular and slotted synthetic jets for flow control in a twin air intake. *Def. Sci. J.*, 2020, **70**(2), 113-121.
doi: 10.14429/dsj.70.13053
13. Duvigneau, R.; Régis, A.; Hay, & Visonneau, M. Optimal location of a synthetic jet on an airfoil for stall control. 2007, 825-833.
doi: 10.2514/6.2006-3679
14. Duvigneau, R. and Visonneau, M. Optimization of a synthetic jet actuator for aerodynamic stall control. *Computers and Fluids*, 2006, **35**(6), 624-638.
doi: 10.1016/j.compfluid.2005.01.005
15. Kim, S.H. & Kim, C. Separation control on NACA23012 using synthetic jet. *Aerospace Sci. Technol.*, 2009, **13**(4-5), 172-182.
doi: 10.1016/j.ast.2008.11.001
16. Nishibe, K.; Nomura, Y.; Noda, K.; Ohue, H. & Sato, K. Influence of stroke on performance characteristics of synthetic jet fan. *J. Applied Fluid Mech.,* 2018, **11**(4), 945-956.
doi: 10.29252/jafm.11.04.28493
17. Feng, J.; Lin, Y.; Zhu, G. & Luo, X. Effect of synthetic jet parameters on flow control of an aerofoil at high Reynolds number. *Sādhanā*, 2019, **44**(8), 190.
doi: 10.1007/s12046-019-1173-2
18. Ansys: Ansys Fluent- CFD Software. Ansys Inc., 2016.
19. Gil, P. Bluff body drag control using synthetic jet. *J. Applied Fluid Mech.*, 2019, **12**(1), 293-302.
doi: 10.29252/jafm.75.253.28960
20. Smith, B. L. & Swift, G. W. A comparison between synthetic jets and continuous jets. *Experiments in Fluids*, 2003, **34**(4), 467-472.
doi: 10.1007/s00348-002-0577-6
21. Spalart, P. & Allmaras, S. A one-equation turbulence model for aerodynamic flows. *In* 30th aerospace sciences meeting and exhibit (p. 439), (1992, January).
doi: 10.2514/6.1992-439
22. Rumsey, C. Successes and challenges for flow control simulations. *In* 4th flow Control Conference (p.4311) (2008, January).
doi: 10.1260/1756-8250.1.1.1
23. Rumsey, C.L.; Gatski, T.B.; Sellers III, W.L.; Vasta, V.N. and Viken, S.A. Summary of the 2004 computational fluid dynamics validation workshop on synthetic jets. *AIAA Journal*, 2006, **44**(2), 194-207.
doi: 10.2514/1.12957
24. Seifert, A.; Greenblatt, D. & Wygnanski, I. J. Active separation control: An overview of Reynolds and mach numbers effects. *Aerospace Sci. Technol.*, 2004, **8**(7), 569-582.
doi: 10.1016/j.ast.2004.06.007

CONTRIBUTORS

Mr Deepak Kumar Singh completed MTech (Fluids Engineering) from MNNIT Allahabad. He specialises in fluid mechanics and CFD and has published a few research papers in aerodynamics in refereed journals and international conferences. He is currently pursuing PhD from IIT Delhi.
Contribution in the current study: He carried out the CAD modelling, CFD analysis and wrote the first draft of the paper.

Dr Anuj Jain has completed his PhD in Chemical Engineering from IIT Roorkee. Currently he is a Professor at the Department of Applied Mechanics, MNNIT Allahabad, India. He has over 30 years of research experience in thermo-fluid flows, multiphase flows and bio-fluid dynamics and has published over 150 research articles in peer-reviewed journals and reputed conferences in India and abroad. He served at various academic and administrative positions during his career, authored two textbooks, supervised numerous MTech and PhD theses and handled three government sponsored research projects.
Contribution in the current study: He acted as an advisor to the research work reported in the paper.

Dr Akshoy Ranjan Paul has received BTech and MTech in Mechanical Engineering, while did PhD from MNNIT Allahabad. He is an Associate Professor at the Department of Applied Mechanics, MNNIT Allahabad, India and is involved in teaching and research for 19 years. He has published over 150 research papers on fluid dynamics, flow control, CFD and green energy and wrote four textbooks. He is the reviewer of many journals and conducted various conferences, workshops, short-term courses on a plethora of topics. He is involved in six externally funded research projects so far.
Contribution in the current study: He worked with the first author, advised him regarding CFD computation and has also revised the draft of the manuscript to make it final.